Korean J. Chem. Eng., **28**(7), 1599-1607 (2011)
DOI: 10.1007/s11814-011-0003-y

Hydrodynamic modeling of the entrainment of Geldart A group particles in gas-solid fluidized bed: The effect of column diameter

Mehdi Azadi†

Department of Chemical Engineering, College of Engineering, Shahid Bahonar University of Kerman, Kerman, Iran
(*Received 13 July 2010 • accepted 3 January 2011*)

Abstract−A multi-fluid Eulerian computational fluid dynamics (CFD) model is used to simulate the entrainment of fluid catalytic cracking (FCC) particles in gas-solid fluidized beds. Entrainment of Geldart A group particles was studied because of their wide range of industrial use. The model was based on the kinetic theory of granular flow. The CFD model was used to investigate the effect of column diameter on the entrainment flux of particles in a binary mixture. Two different sizes of particles were used because many engineering applications deal with binary mixture of particles in fluidized beds. Various column diameters, including 38 mm, 76 mm, 114 mm, 152 mm, and 190 mm, were investigated. The entrainment flux of particles was increased with decreasing column diameter. The effect of column diameter was not significant for column diameters larger than 114 mm. Furthermore, increasing the superficial gas velocity increased the entrainment flux of particles. Model predictions were also compared with experimental findings.

Key words: Entrainment, Fluidized Bed, CFD, Column Diameter, FCC

INTRODUCTION

Entrainment is a process which might occur in fluidized beds to carry particles over the bed by means of fluid flow. Entrainment flux of particles has to be known for the design of an appropriate gas-solid separator such as cyclone or filter. Furthermore, the entrainment of particles out of the bed is a disadvantage in fluidized bed reactors in many industrial applications. Entrainment can occur in fluidized bed reactors for Geldart A group particles, like fluid catalytic cracking (FCC), which are widely used in chemical industries.

With the recent development of mathematical modeling, numerical simulation becomes a new tool to study and predict the hydrodynamics of multiphase flows [1-3]. In this regard, computational fluid dynamics (CFD) modeling has proved to be a promising tool in the analysis of gas and particulate systems. CFD is specially efficient for multi-particle modeling of fluidized beds.

In recent years, considerable researches have been carried out to utilize computational fluid dynamics for modeling of gas-solid fluidized beds [4-6]. Two different classes of computational fluid dynamic models are used for modeling of fluidized beds: Eulerian-Lagrangian model and Eulerian-Eulerian model [7].

In Lagrangian models, the equation of motion is solved for each individual particle, taking into account interactions with other particles and continuous phase. In Eulerian models, all phases are modeled as fully interpenetrating continua. The Eulerian-Eulerian model is an appropriate model to simulate gas-solid fluidized beds [8,9]. The Eulerian model's application to describe the fluid dynamics of fluidized beds was reported by Refs. [10-14].

Eulerian-Eulerian models need further closure laws to describe the rheology of solid phase [15]. Most of the recent models use the kinetic theory of granular flow to obtain constitutive equations [16-20]. The kinetic theory of granular flow is based on the analogy between the thermal motion of the gas molecules in the kinetic theory of gases and the random motion of solid particles [21]. Champan and Cowling [21] established the development of kinetic theory of granular flow. It was then extended by Jenkins and Savage [16], Lun et al. [17] and Johansen and Jackson [22]. The kinetic theory of granular flow was used by Sinclair and Jackson [23] for multiphase modeling for the first. However, it has become a very promising tool for modeling of gas-particulate fluidized beds.

In this research, a multi-fluid Eulerian model based on the kinetic theory of granular flow is established to investigate the effect of column diameter on the entrainment of Geldart A group particles from a binary mixture in a gas-solid fluidized bed. Column diameters of 38 mm, 76 mm, 114 mm, 152 mm, and 190 mm were compared with the model. The effect of superficial gas velocity was also studied with the model. The numerical predictions were compared with the experimental data of Tasirin and Geldart [24] to evaluate the performance of the model.

FLUID DYNAMIC MULTI-FLUID MODEL

An Eulerian-Eulerian modeling method is used to study the entrainment of Geldart A group particles in gas-solid fluidized bed in the current research. The model involves the kinetic theory of granular flow to obtain constitutive equations. Viscous forces and solid pressure of the solid phases can be described as a function of granular temperature, by taking advantage of the kinetic theory of granular flow [4,23]. No mass transfer was allowed between phases. The model used in this study is described as follows.

Continuity equations

Gas phase

$$\frac{\partial}{\partial t}(\varepsilon_g \rho_g) + \nabla \cdot (\varepsilon_g \rho_g \vec{v}_g) = 0 \quad (1)$$

†To whom correspondence should be addressed.
E-mail: Mehdi.azadi83@gmail.com

Solid phase

$$\frac{\partial}{\partial t}(\varepsilon_s\rho_s)+\nabla\cdot(\varepsilon_s\rho_s\vec{v}_s)=0 \quad (2)$$

where ε, ρ and v are volume fraction, density and velocity respectively.

Momentum equations

The momentum equation for gas and solid phases

Gas phase:

$$\frac{\partial}{\partial t}(\varepsilon_g\rho_g\vec{v}_g)+\nabla\cdot(\varepsilon_g\rho_g\vec{v}_g\vec{v}_g)=-\nabla p+\nabla\cdot\bar{\bar{\tau}}_g+\varepsilon_g\rho_g\vec{g}+\sum_{s=1}^{N}k_{gs}(\vec{v}_s-\vec{v}_g) \quad (3)$$

where p and $\vec{g}$ are gas pressure and gravity, respectively.

k_{gs} is gas-solid momentum exchange coefficient of gas and solid phase, $\nabla\cdot\bar{\bar{\tau}}_g$ is gas phase tensor.

Solid phase (s=1, 2, …, N)

$$\frac{\partial}{\partial t}(\varepsilon_s\rho_s\vec{v}_s)+\nabla\cdot(\varepsilon_s\rho_s\vec{v}_s\vec{v}_s)=\nabla\cdot\bar{\bar{\tau}}_s+\varepsilon_s\rho_s\vec{g}+k_{gs}(\vec{v}_g-\vec{v}_s)+\sum_{n=1,s\neq n}^{N}k_{ns}(\vec{v}_n-\vec{v}_s) \quad (4)$$

where k_{ns}, is solid-solid exchange coefficient and τ_s is solid phase stress tensor.

Gas phase stress tensor

$$\bar{\bar{\tau}}_g=\varepsilon_g\mu_g[\nabla\cdot\vec{v}_g+\nabla\cdot\vec{v}_g^{T}]-\frac{2}{3}\varepsilon_g\mu_g\nabla\cdot\vec{v}_g \quad (5)$$

Solid phase stress tensor of phase s

$$\bar{\bar{\tau}}_s=-P_s\bar{\bar{I}}+\varepsilon_s\mu_s(\nabla\cdot\vec{v}_s+\nabla\cdot\vec{v}_g^{T})+\varepsilon_s\left(\lambda_s-\frac{2}{3}\mu_s\right)\nabla\cdot\vec{v}_s\bar{\bar{I}} \quad (6)$$

where μ_s and λ_s are solid shear viscosity and bulk viscosity, respectively.

Solid shear viscosity

$$\mu_s=\mu_{s,col}+\mu_{s,kin}+\mu_{s,fr} \quad (7)$$

Collisional viscosity

$$\mu_{s,col}=\frac{4}{5}\varepsilon_s^2\rho_s d_s g_{0,ss}(1+e_{ss})\left(\frac{\Theta_s}{\pi}\right)^{1/2} \quad (8)$$

where $g_{0,ss}$ is radial distribution, e_{ss} is restitution coefficient, and Θ_s is granular temperature.

Kinetic viscosity [25]

$$\mu_{s,kin}=\frac{\varepsilon_s\rho_s d_s\sqrt{\Theta_s\pi}}{6(3-e_{ss})}\left[1+\frac{2}{5}(1+e_{ss})(3e_{ss}-1)\varepsilon_s g_{0,ss}\right] \quad (9)$$

Frictional viscosity [26]

$$\mu_{s,fr}=\frac{P_s\sin\phi}{2\sqrt{I_{2D}}} \quad (10)$$

where P_s is the solid pressure, ϕ is the angle of the internal friction and I_{2D} is the second invariant of the deviatoric stress tensor

Solid bulk viscosity [17]

$$\lambda_s=\frac{4}{3}\varepsilon_s^2\rho_s d_s g_{0,ss}(1+e_{ss})\left(\frac{\Theta_s}{\pi}\right)^{1/2} \quad (11)$$

Solid pressure

A general model for the solids pressure in the presence of several solid phases by Gidaspow [5]

$$P_s=\varepsilon_s\rho_s\Theta_s+\sum_{n=1}^{N}\frac{\pi}{3}g_{0,ns}d_{sn}^3n_sn_n(1+e_{sn})f(m_n,m_s,\Theta_n,\Theta_s) \quad (12)$$

where $d_{ns}=((d_n+d_s)/2)$ is the average diameter, n_n and n_s are the number of particles, m_n and m_s are the masses of particles in the phase phases n and s, and f is a function of the masses of the particles and their granular temperatures.

However, this equation can be simplified to give the following form [8]:

$$p_s=\varepsilon_s\rho_s\Theta_s+\sum_{p=1}^{N}2\frac{d_{ns}^3}{d_n^3}(1+e_{ns})g_{0,ns}\varepsilon_n\varepsilon_s\rho_s\Theta_s \quad (13)$$

Radial distribution for n solid phases [8]

$$g_{0,ss}=\left[1-\left(\frac{\varepsilon_s}{\varepsilon_{s,max}}\right)^{1/3}\right]^{-1}+\frac{1}{2}d_s\sum_{n=1}^{N}\frac{\varepsilon_n}{d_n} \quad (14)$$

where (n are solids phases)

$$\varepsilon_s=\sum_{n=1}^{N}\varepsilon_n \quad (15)$$

The Syamlal-O'Brien drag model [25]

$$k_{gs}=\frac{3\varepsilon_s\varepsilon_g\rho_g}{4v_{r,s}^2d_s}C_D\left(\frac{Re_s}{v_{r,s}}\right)\left|\vec{v}_s-\vec{v}_g\right| \quad (16)$$

where according to Dalla Valle [27], C_D is defined as

$$C_D=\left(0.63+\frac{4.8}{\sqrt{Re_s/v_{r,s}}}\right)^2 \quad (17)$$

And $v_{r,s}$ is a correlation for the terminal velocity of the solid phase

$$v_{r,s}=0.5(A-0.06Re_s+\sqrt{(0.06Re_s)^2+0.12Re_s(2B-A)+A^2}) \quad (18)$$

With

$$A=\varepsilon_g^{4.14}\ \&\ B=0.8\varepsilon_g^{1.28}\ \text{for}\ \varepsilon_g\le 0.85$$

And

$$A=\varepsilon_g^{4.14}\ \&\ B=\varepsilon_g^{2.65}\ \text{for}\ \varepsilon_g\le 0.85$$

For the particle-particle momentum exchange coefficient the Syamlal-O'Brien-symmetric model [28] was used, which may be written as

$$k_{ns}=\frac{3(1+e_{ns})(\pi/2+c_{fr,ns}\pi^2/8)\varepsilon_s\rho_s\varepsilon_n\rho_n(d_n+d_s)^2g_{0,ns}}{2\pi(\rho_nd_n^3+\rho_sd_s^3)}\times\left|\vec{v}_s-\vec{v}_n\right| \quad (19)$$

where e_{ns} is the restitution coefficient, $C_{fr,ns}$ is the friction coefficient between phases n & s, d_n is the diameter of the particles of the phase n and $g_{0,ns}$ is the radial distribution coefficient.

The kinetic fluctuation energy, which is derived from kinetic theory of granular flow, can be described as the following expression [29]:

$$\frac{3}{2}\left[\frac{\partial}{\partial t}(\rho_s\varepsilon_s\Theta_s)+\nabla\cdot(\rho_s\varepsilon_s\vec{v}_s\Theta_s)\right]=(-p_s\bar{\bar{I}}+\bar{\bar{\tau}}_s):\nabla\vec{v}_s+\nabla\cdot(k_{\Theta_s}\nabla\Theta_s)-\gamma_{\Theta_s}+\phi_{gs} \quad (20)$$

where $(-p_s\bar{\bar{I}}+\bar{\bar{\tau}}_s):\nabla\vec{v}_s$ is the energy generation by solid stress tensor, $k_{\Theta_s}\nabla\Theta_s$ is the energy diffusion, γ_{Θ_s} is the collision dissipation of

energy, and ϕ_{gs} is the transfer of kinetic energy.

The diffusion coefficient of granular energy, k_{Θ_s}, can be described by the Syamlal et al. model [30]

$$k_{\Theta_s} = \frac{15 d_s \rho_s \varepsilon_s \sqrt{\Theta_s \pi}}{4(41-33\eta)}\left[1+\frac{12}{5}\eta^2(4\eta-3)\varepsilon_s g_{0,ss} + \frac{16}{15\pi}(41-33\eta)\eta\varepsilon_s g_{0,ss}\right] \quad (21)$$

Where

$$\eta = \frac{1}{2}(1+e_{ss})$$

The dissipation energy of particles by collisions, γ_{Θ_s}, which presents the rate of energy dissipation of the s^{th} solid phase because of particle-particle collisions, is described with the following expression by Lun et al. [17]:

$$\gamma_{\Theta m} = \frac{12(1-e_{ss}^2) g_{0,ss}}{d_s\sqrt{\pi}} \rho_s \varepsilon_s^2 \Theta_s^{3/2} \quad (22)$$

The kinetic energy transfer of random fluctuations in particle velocity is represented by ϕ_{gs} [31]

$$\phi_{gs} = -3K_{gs}\Theta_s \quad (23)$$

1. Simulation Procedure

The numerical solution for governing equations was provided with a CFD based code (Fluent 6.3.26). The second-order upwind differencing scheme was used as the discretization method. Discretization is a process which changes the partial differential equations of the model to algebraic equations for numerical solution. The phase coupled SIMPLE (PCSIMPLE) algorithm by Vasquez and Ivanov [32], which is an extension of SIMPLE algorithm by Patankar [33], was used for pressure-velocity coupling.

A schematic drawing of the simulated gas-solid fluidized bed is shown in Fig. 1. The multi-fluid model consisted of three phases: air as the primary phase (gas phase), small and large FCC particles as the secondary phases (solid phases). Two-dimensional computational grids were generated in radial and axial directions to study

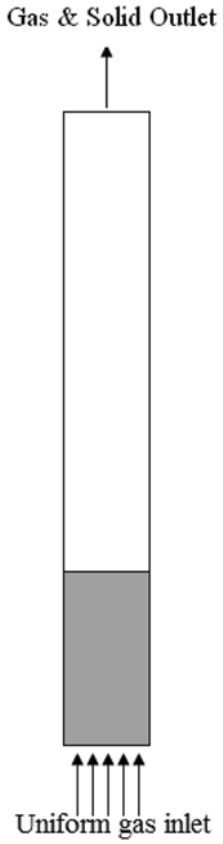

Fig. 1. A schematic drawing of the 2-D gas-solid fluidized bed.

Table 1. Simulation settings for the CFD model

Description	Value/Settings	Additional comments
Column height	2.4 m	Fixed
Column diameter	38, 76, 114, 152, 190 mm	Compared diameters
Static bed height	0.15 m	Fixed
Large particles		
Diameter	140 μm	Uniform
Density	1,180 kg/m^3	FCC (Geldart A group)
Volume fraction	0.44	Fixed
Small particles		
Diameter	45 μm	Uniform
Density	1,350 kg/m^3	FCC (Geldart A group)
Volume fraction	0.11	Fixed
Superficial gas velocity	0.4, 0.5, 0.6, 0.7, 0.8 m/s	Compared velocities
Gas viscosity	1.85×10^{-5} kg/ms	Fixed
Gas density	1.225 kg/m^3	Air
Gravity acceleration	9.81 m/s^2	Fixed
Time step size	0.001 s	Fixed
Maximum iterations per time step	100	Fixed
Inlet boundary condition	Velocity inlet	Superficial gas velocity
Outlet boundary condition	Pressure outlet	Fully developed flow

the entrainment of particles. A cell growth factor was applied to meshes in radial direction to generate a higher density of grids approaching to the bed side walls to consider a higher restriction for computations in this important region. The computational meshes consisted of approximately 30,000 to 35,000 cells. Using higher grid resolutions did not affect the results, which confirms the grid independency of the simulations. A convergence criterion of 0.0001 was considered for the relative error between two successive iterations. The simulation durations varied from 10 to 40 s for the superficial gas velocities of 0.4 to 0.8 m/s. The computations were performed on a 2.8 GHz CPU and 4 GB of RAM workstation. A summary of the simulation settings is presented in Table 1.

RESULTS AND DISCUSSION

1. Model Validation

The simulation results were compared with the experimental data achieved by Tasirin and Geldart [24] to evaluate the applicability of the model. The fluidized beds' properties, reported by Tasirin and Geldart [24], which are used in this study, are presented in Table 2. Fig. 2 compares the model predictions with the experimental data for the column diameter of 76 mm. The modeling results show good agreement with experimental findings for the entrainment flux of particles at different superficial velocities. Fig. 3 offers a comparison of the simulation results with the experimental data for the column diameter of 152 mm. Comparison of the entrainment rate of particles at different gas velocities for simulated and experimental achievements is presented in this figure, which confirms the validation of the model.

Table 2. Fluidized beds' properties by Tasirin and Geldart [24]

Property	Value
Bed diameter (mm)	76, 152
Bed height (m)	2.4
Particle size (μm)	45, 140
Particle type	FCC (Geldart A group)

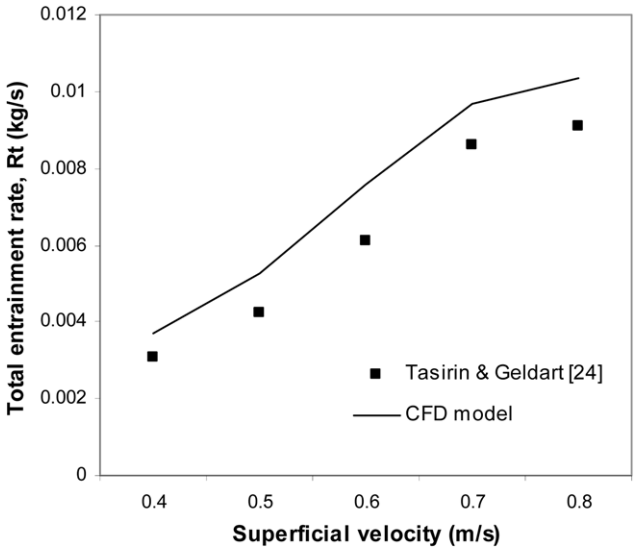

Fig. 3. Comparison of the simulation results with experimental data for the column diameter of 152 mm.

2. Effect of Bed Diameter

Entrainment flux of Geldart A group particles was calculated for different column diameters of 38 mm, 76 mm, 114 mm, 152 mm, and 190 mm at various superficial velocities to evaluate the effect of bed diameter. Fig. 4 compares the calculated entrainment fluxes for different bed diameters at various superficial gas velocities. It was observed that the entrainment flux of particles decreased with increasing the bed diameter. However, minor changes of entrainment flux were observed for higher column diameters. As shown in Fig. 4, the changes in the entrainment flux of particles were more significant between column diameters of 38 mm, 76 mm, and 114 mm, whereas, increasing the column diameter to 152 mm and 190 mm did not change the entrainment flux as significantly as the previous changes for smaller bed diameters. This fact is caused by the wall effect, which affects the gas velocity regime in the cross-section

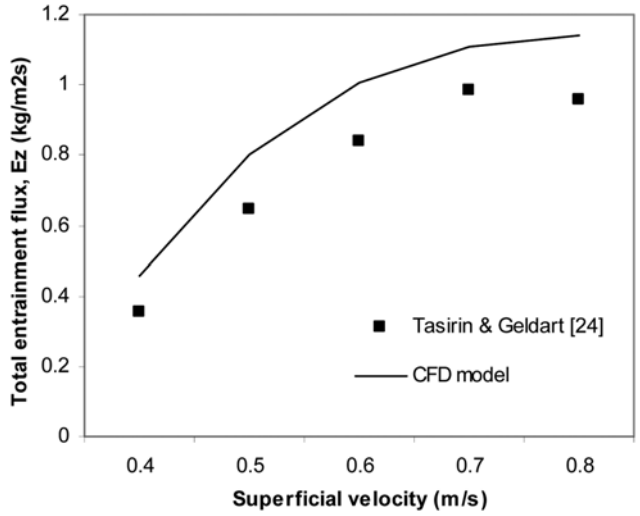

Fig. 2. Comparison of the model predictions with experimental data for the column diameter of 76 mm.

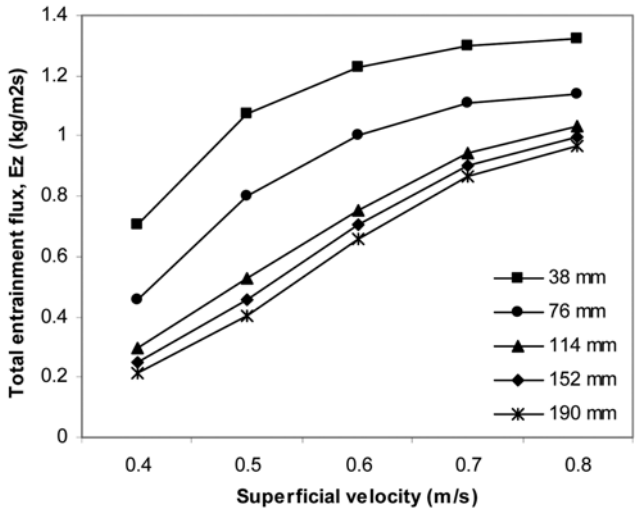

Fig. 4. Comparison of the calculated entrainment fluxes for different bed diameters at various superficial gas velocities.

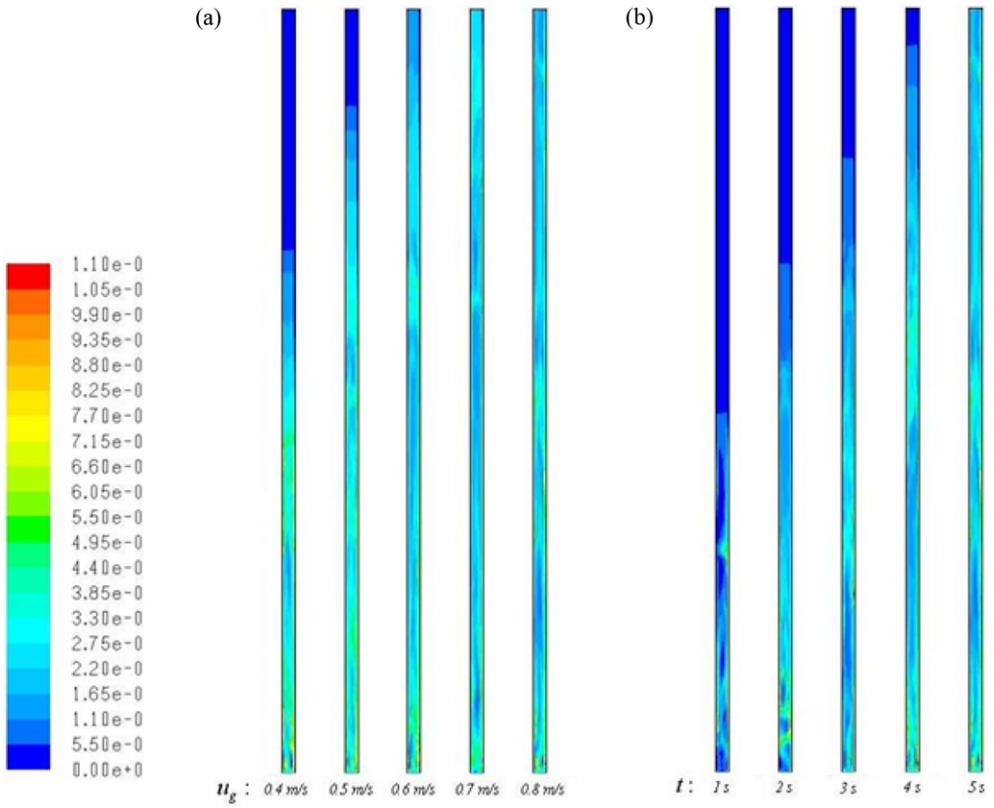

Fig. 5. Volume fraction distribution of small FCC particles for column diameter of 38 mm at (a) different superficial velocities, (b) the first 5 seconds of the process for the superficial velocity of 0.7 m/s.

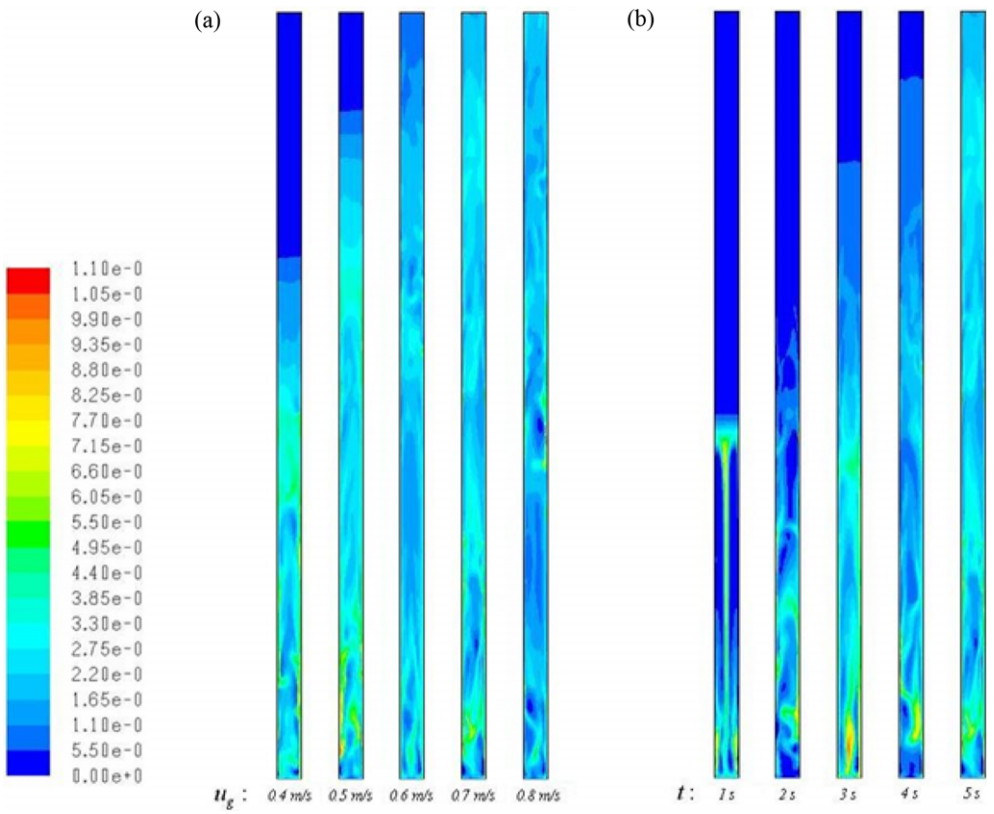

Fig. 6. Volume fraction distribution of small FCC particles for column diameter of 76 mm at (a) different superficial velocities, (b) the first 5 seconds of the process for the superficial velocity of 0.7 m/s.

of fluidized bed. This finding is in agreement with those of other authors [34-36,24] that there was little change of entrainment flux for column diameters above 0.1 m.

Figs. 5, 6, 7, 8, and 9 show the calculated volume fraction distribution of small FCC particles for different column diameters of 38 mm, 76 mm, 114 mm, 152 mm, and 190 mm, respectively. The

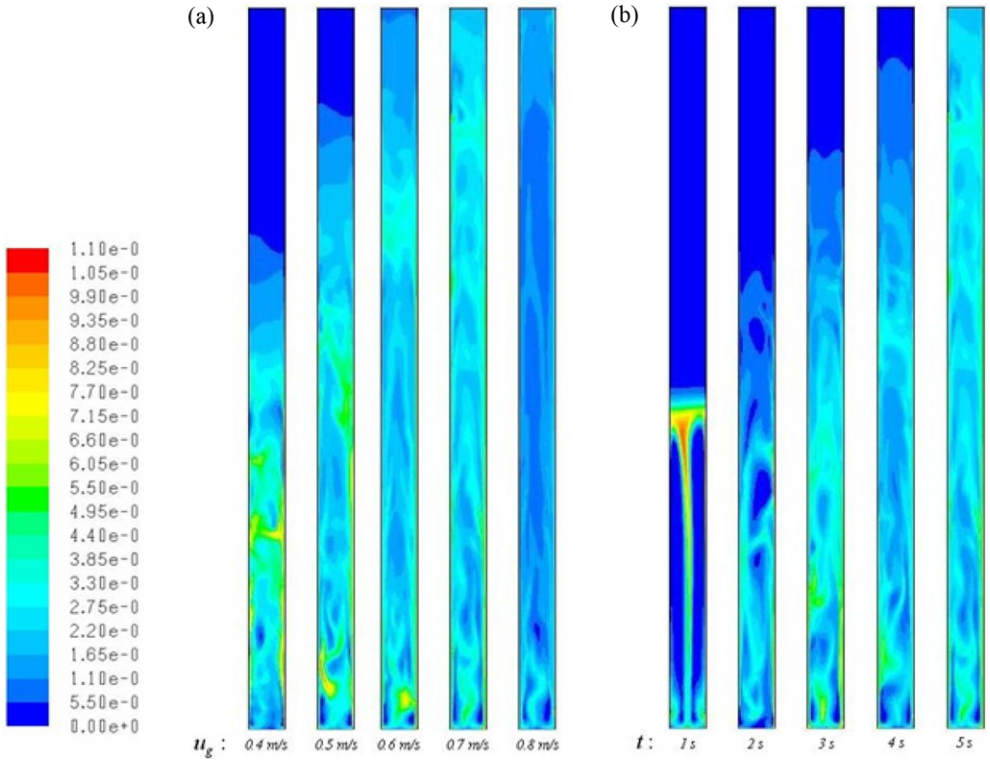

Fig. 7. Volume fraction distribution of small FCC particles for column diameter of 114 mm at (a) different superficial velocities, (b) the first 5 seconds of the process for the superficial velocity of 0.7 m/s.

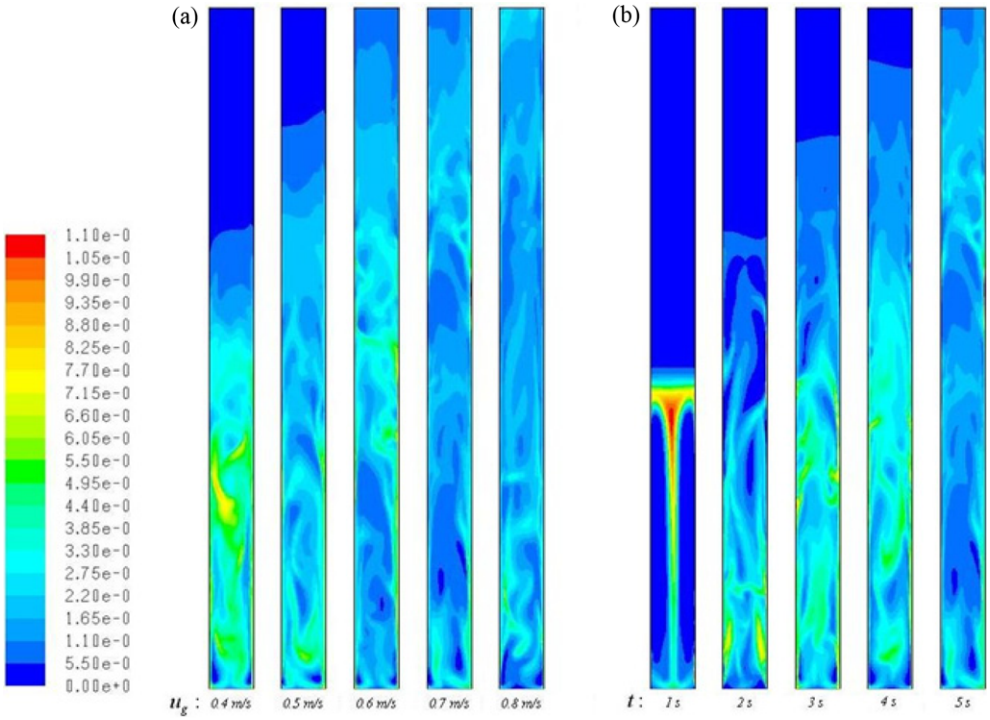

Fig. 8. Volume fraction distribution of small FCC particles for column diameter of 152 mm at (a) different superficial velocities, (b) the first 5 seconds of the process for the superficial velocity of 0.7 m/s.

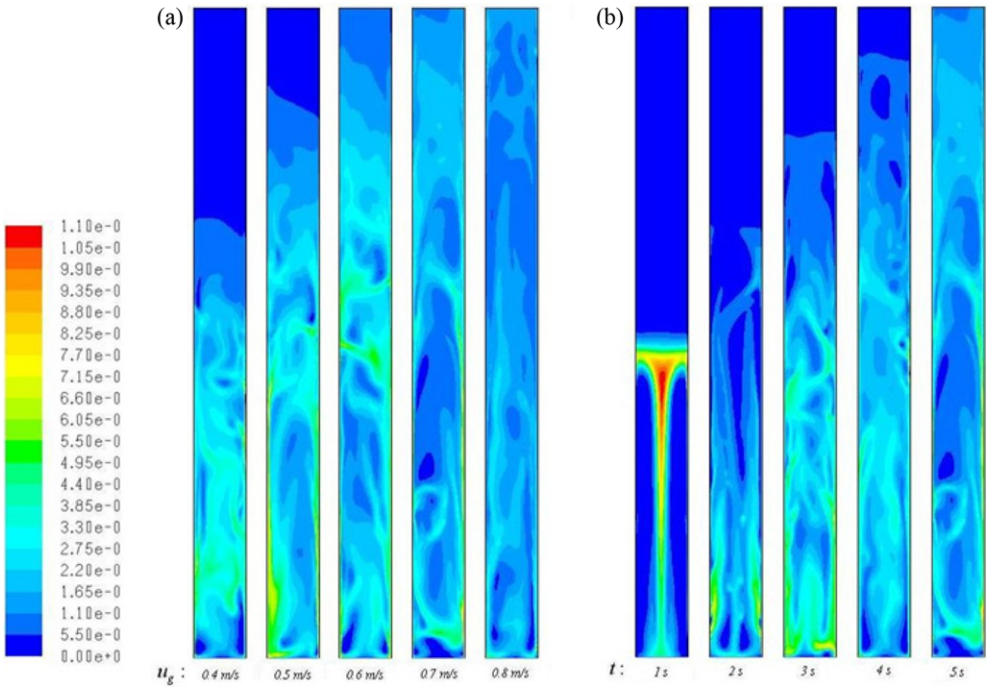

Fig. 9. Volume fraction distribution of small FCC particles for column diameter of 190 mm at (a) different superficial velocities, (b) the first 5 seconds of the process for the superficial velocity of 0.7 m/s.

distribution of particles for different column diameters at different superficial gas velocities is presented in these figures. Superficial gas velocity is considered as a determining factor for the entrainment of particles. As shown in Figs. 5(a)-9(a), the entrainment of particles increased with increasing the superficial gas velocities. Kato et al. [37] and Nakagawa et al. [38] reported that superficial gas velocity significantly affected the entrainment of particles.

3. Hydrodynamic Behavior

The hydrodynamics of the first five seconds of the process for the gas velocity of 0.7 m/s can be studied with Figs. 5(b)-9(b). To improve our understanding of the complicated hydrodynamic behavior of the particles, the radial distribution of small FCC particles was calculated. Fig. 10 presents the radial profile of small particles' volume fraction for the column diameter of 76 mm and superficial gas velocity of 0.7 m/s at z=1.75 m. It shows that the solid concentration has the highest value near the wall region and decreases along the radial direction to the center of the bed. The velocity profile of the particles is a term which changes with respect to the column diameter and is related to the particle entrainment flux. Fig. 11 compares the velocity profiles of small particles for 76 mm and 152 mm diameter columns at z=1.75 m with inlet superficial velocity of 0.7 m/s. It was revealed that the maximum velocities were higher in

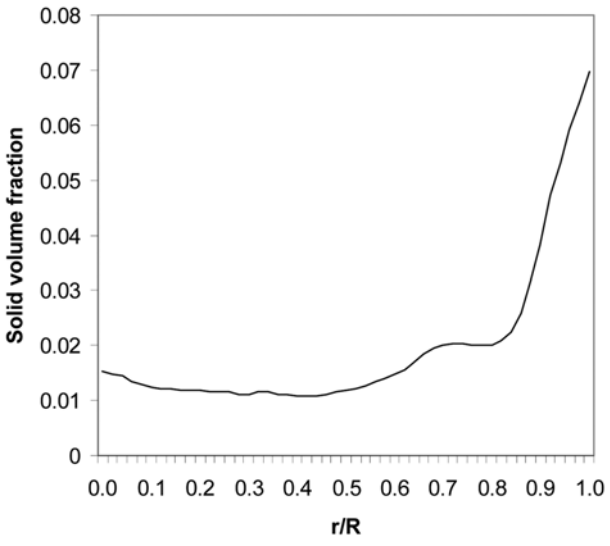

Fig. 10. Radial profile of small FCC particles' volume fraction for the column diameter of 76 mm and superficial gas velocity of 0.7 m/s at z=1.75 m.

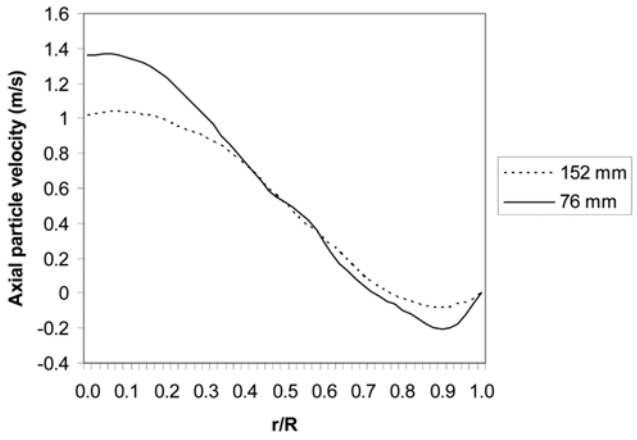

Fig. 11. Comparison of the velocity profiles of small FCC particles for 76 mm and 152 mm diameter columns at z=1.75 m.

smaller bed diameters, which results in the higher entrainment flux of particles for smaller column diameters.

CONCLUSIONS

An Eulerian-Eulerian computational fluid dynamics model, based on the kinetic theory of granular flow, was developed to simulate the complex hydrodynamics of gas-particulate flow in fluidized beds. The model was used to investigate the effect of column diameter on entrainment of Geldart A group particles from a binary mixture in a gas-solid fluidized bed. Furthermore, the CFD model was used to study the effect of superficial gas velocity and the hydrodynamic behavior of a gas-solid fluidized bed. The model showed that the entrainment flux of particles was reduced with increasing the column diameter, although the effect of bed diameter was found to be more significant for smaller column diameters. The superficial velocity showed to have a major effect on the process, as the entrainment flux of particles increased with increasing the gas velocity. The modeling predictions were in good agreement with experimental data, which confirms the applicability of the model.

NOMENCLATURE

C_D : drag coefficient, dimensionless
$C_{fr,i}$: friction coefficient
d_i : diameter [m]
e_{ss} : restitution coefficient, dimensionless
g : gravity [m/s^2]
$g_{0,ss}$: radial distribution coefficient
$\bar{\bar{I}}$: stress tensor
I_{2D} : second invariant of the deviatoric stress tensor
K_{gs} : gas-solid momentum exchange coefficient
$k_{\Theta s}$: diffusion coefficient of granular energy [kg/s m]
m_i : mass of particles [kg]
n_i : number of particles
p : fluid pressure [pa]
P_s : solid pressure [pa]
Re : Reynolds number
t : time [s]
v_i : velocity [m/s]

Greek Letters

ε_i : volume fracion
Θ_i : granular temprature [m^2/s^2]
λ_i : bulk viscosity [kg/s m]
μ_i : shear viscosity [kg/s m]
ρ_i : density [kg/m^3]
$\bar{\bar{\tau}}_i$: stress tensor [pa]
$\gamma_{\Theta m}$: collision dissipation of energy [kg/s^{3}m]
ϕ_{gs} : transfer rate of kinetic energy [kg/s^{3}m]
ϕ : angle of the integral friction
η : effectiveness factor

REFERENCES

1. J. D. Chung, J. W. Kim and Y. M. Park, *Korean J. Chem. Eng.*, **27**(1), 83 (2010).
2. L. Fan, R. Hai and Z. Lu, *Korean J. Chem. Eng.*, **26**(5), 1272 (2009).
3. M. Azadi, M. Azadi and A. Mohebbi, *J. Hazard. Mater.*, **182**, 835 (2010).
4. D. Gidaspow, *Multiphase flow and fluidization: Continuum and kinetic theory descriptions*, Academic Press, Boston (1994).
5. J. L. Sinclair, *Hydrodynamic modelling*, In: Grace, J. R., Avidan, A. A. and Knowlton, T. M. (Eds.), Circulating Fluidized Beds, Blackie, London (Chapter 5) (1997).
6. B. G. M. van Wachem and A. E. Almstedt, *Chem. Eng. J.*, **96**, 81 (2003).
7. C. Crowe, M. Sommerfield and Y. Tsuji, *Multiphase flows with droplets and particles*, CRC Press, London (1998).
8. Fluent user manual, Fluent Inc. (2006).
9. C. C. Pain, S. Mansoorzadeh and C. R. E. de Oliveira, *Int. J. Multiphas. Flow*, **27**, 527 (2001).
10. J. A. M. Kuipers, K. J. van Duin, F. P. H. van Beckum and W. P. M. Van Swaaij, *Chem. Eng. Sci.*, **47**, 1913 (1992).
11. V. Mathiesen, T. Solberg and B. H. Hjertager, *Int. J. Multiphas. Flow*, **26**(3), 387 (2000).
12. S. Benyahia, H. Arastoopour and T. M. Knowlton, *Chem. Eng. Commun.*, **189**(4), 510 (2001).
13. D. Gera, M. Gautam, Y. Tsuji, T. Kawaguchi and T. Tanaka, *Powder Technol.*, **98**, 38 (1998).
14. A. Almuttahar and F. Taghipour, *Chem. Eng. Sci.*, **63**, 1696 (2008).
15. L. Huilina, H. Yurong and D. Gidaspow, *Chem. Eng. Sci.*, **58**, 1197 (2003).
16. J. T. Jenkins and S. B. Savage, *J. Fluid Mech.*, **130**, 187 (1983).
17. C. K. K. Lun, S. B. Savage, D. J. Jeffrey and N. Chepumiy, *J. Fluid Mech.*, **140**, 223 (1984).
18. M. W. Richman, *J. Rheol.*, **33**, 1293 (1989).
19. D. L. Koch, *Phys. Fluids*, **A2**, 1711 (1990).
20. J. M. Montanero, V. Garzo, A. Santos and J. J. Brey, *J. Fluid Mech.*, **389**, 391 (1999).
21. S. Chapman and T. Cowling, *The mathematical theory on non-uniform gases*, Cambridge University Press, Cambridge (1970).
22. P. Johnson and R. Jackson, *J. Fluid Mech.*, **176**, 67 (1987).
23. J. Sinclair and R. Jackson, *AIChE J.*, **35**, 1473 (1989).
24. S. M. Tasirin and D. Geldart, *Powder Technol.*, **95**, 240 (1998).
25. M. Syamlal and T. J. O'Brien, *Computer simulation of bubbles in a fluidized bed*, AIChE Symp. Ser., **85**, 22 (1989).
26. D. G. Schaeffer, *J. Diff. Eq.*, **66**, 19 (1987).
27. J. M. Dalla Valle, Micromeritics, Pitman, London (1948).
28. M. Syamlal, *The particle-particle drag term in a multiparticle model of fluidization*, National Technical Information Service, Springfield, VA, (1987).
29. J. Ding and D. Gidaspow, *AIChE J.*, **36**, 523 (1990).
30. M. Syamlal, W. Rogers and T. J. O'Brien, MFIX Documentation: Volume 1, Theory Guide. National Technical Information Service, Springfield, VA, DOE/METC-9411004, NTIS/DE9400087 (1993).
31. D. Gidaspow, R. Bezburuah and J. Ding, *Hydrodynamics of Circulating Fluidized Beds*, Kinetic Theory Approach, In Fluidization VII, Proceedings of the 7th Engineering Foundation Conference on Fluidization, 75 (1992).
32. S. A. Vasquez and V. A. Ivanov, *A Phase Coupled Method for Solving Multiphase Problems on Unstructured Meshes*, In Proceedings of ASME FEDSM'00: ASME 2000 Fluids Engineering Division Summer Meeting, Boston, June (2000).

33. S. Patankar, *Numerical heat transfer and fluid flow*, Hemisphere, Washington, D.C. (1980).
34. W. K. Lewis, E. R. Gilliland and P. M. Lang, *Entrainment from fluidized beds*, Chem. Eng. Prog. Symp. Ser., **58**, 65 (1962).
35. M. Colakyan and O. Levenspiel, *Powder Technol*., **38**, 223, (1984).
36. W. Wohlfarth, in D. Geldart (Ed.), Gas Fluidization Technology, Wiley, Chichester, UK, 141 (1986).
37. K. Kato, S. Kanbara, T. Tajima, H. Shibasaki, K. Ozawa and T. Takarada, *J. Chem. Eng. Jpn*., **20**, 498 (1987).
38. N. Nakagawa, S. Arita, H. Uchida, N. Takamura, T. Takarada and K. Kato, *J. Chem. Eng. Jpn*., **27**, 79 (1996).